Performance of Widely Tunable Multi-Quantum-Well and Bulk Laser Diodes and the Main Limiting Factors

Georgios Kyritsis and Nick Zakhleniuk

Abstract—The output power and tuning performance of multi-quantum-well (MQW) and bulk InGaAsP/InP-distributed Bragg reflector (DBR) tunable laser diodes (TLDs) are investigated over a wide wavelength tuning range using physics-based PICS3D and VPI laser simulation tools within the travelling-wave formalism. The key result of our simulations is the discovery of a new effect in TLDs due to intervalence band absorption (IVBA) in passive phase and DBR sections, which limits the wavelength tuning range. The physical mechanism responsible for such a behavior is a collapse of the spectral-mode selectivity by the DBR due to large IVBA losses in the phase or/and DBR sections. We fundamentally demonstrate different roles played by the IVBA in the active and passive sections of a TLD. It is shown that the IVBA in passive sections and the carrier relaxation broadening (CRB) of the Lorentzian lineshape function in the lasers' active and passive sections play a crucial role in TLD tuning operation. The IVBA coefficient k_{IVBA} and the intraband relaxation time τ_{in} are the major limiting factors that define the output power variation and the achievable tuning range of the lasers. Both bulk and MQW lasers with small k_{IVBA} demonstrate a wide wavelength tuning range above 30 nm, while for large k_{IVBA}, the tuning range drops below 10 nm. We show that the output power variation with tuning due to the CRB parameter τ_{in} is qualitatively different in bulk and MQW TLDs. The TLD tuning and power performance is also strongly affected by the shapes of the net gain and the cavity mirror loss spectra and their mutual positioning with respect to the lasing cavity mode during the tuning. The limiting parameters k_{IVBA} and τ_{in} as well as gain and mirror loss spectra must be thoroughly evaluated in each TLD structure prior to the device design and optimization in order to achieve the best performance in terms of the wavelength tuning and the output power stability.

Index Terms—Semiconductor lasers, tunable laser diode, intervalence band absorption, Lorentzian lineshape, electron relaxation broadening, gain spectra, simulation, PICS3D, VPI.

I. Introduction

TUNABLE laser diodes (TLDs) are important components for optical transmission systems and have many practical applications, especially in modern high-speed networks and wavelength-division-multiplexing (WDM) lightwave systems. The key aspects of their operation are the high spectral purity,

very accurate mode selection, wide tuning range, high optical output power, and narrow spectral linewidth. Various contributions of TLDs to the improvement and optimisation of modern optical networks have been well documented [1]–[3].

The TLD output power stability during wavelength tuning is one of the most important factors for adequate laser operation in optical transmission systems and is sought at all times. The main effect which disrupts this stability and usually leads to power decrease is the existence of losses in the tuning sections. These losses are either internal losses of the tuning region medium or they are caused by free-carrier absorption (FCA) and intervalence band absorption (IVBA). The FCA and IVBA losses produce even more problems because they vary during the wavelength tuning. This takes place because both the FCA and IVBA are proportional to the carrier density in the tuning regions which increases under the current injection.

The impact of absorption losses on the laser power performance was discussed in the literature for wavelength tunable distributed Bragg reflector (DBR) and distributed feedback (DFB) lasers [4]–[14]. In order to compensate power loss in the tuning sections the most common method is to inject more current into the gain section throughout the tuning process as in [4]. The other proposals include using a thermal tuning method which has advantages of power and linewidth stability, as was first investigated in [5] and [6], although this tuning method is very slow, or inserting a thin layer of active material into the tuning regions in order to generate some gain there which would balance the absorption loss in these regions [7], or special bandgap engineering by selecting the tuning layer bandgap wavelength ($\lambda_g = 1.48$ μm) very close to that of the active region (AR) layer ($\lambda_g = 1.56$ μm), so that the gain spectra of the active and the passive regions overlap due to the bandgap tail states in the tuning region, thus providing an additional gain contribution to the emission spectrum [8].

Some theoretical works on TLDs are based on the rate equation model [9] which reveals no actual information about the gain spectrum shape and its interplay with the cavity lasing mode during tuning. The other models [10] assume for simplicity a broad flat gain spectrum. In real photonic devices though the gain spectrum profile is more complex, especially in multiple quantum-well (MQW) lasers. There are some exceptions, as in [11], where an approximate power expansion up to the cubic terms of the modal gain spectra was used for a particular two-section TLD design, and near 50% power decrease with tuning has been observed.

In this paper it will be shown that the main limiting factors which affect the TLD wavelength tuning and the output power variation during the tuning are the IVBA losses in the passive sections and the intraband relaxation time which defines the lineshape broadening in AR and passive sections [15]. Apart from the IVBA losses, the TLD tuning and output power performance is also strongly affected by the shapes of the gain and cavity mirror loss spectra and their mutual positioning with respect to the longitudinal lasing mode. It will also be demonstrated that power stabilisation can be achieved during continuous tuning with specific gain spectrum shapes and a careful selection of tuning currents. For this purpose, two 3D simulation designs of three-section InGaAsP/InP TLDs operating at 1550 nm CW have been investigated, one with a bulk AR and one with a MQW AR. A comparison of the power performance of these two models under various tuning regimes will be made and the key differences highlighted. The obtained theoretical and simulation results will be applied to explain previously observed experimental data in widely-tunable multi-section lasers with various designs of tuning sections. We use the commercial software Crosslight PICS3D [16] which is widely exploited in laser modelling [17], [18]. The basic device structure, theory, and physical and computational models used in PICS3D are discussed in detail in [19].

One of the main factors which affect the shape of the gain spectrum is the intraband carrier relaxation due to various scattering mechanisms. This causes spectrum broadening and deforms and reduces its peak values [20], [21]. The effect becomes particularly strong in the case of MQW lasers [22]–[25] where the gain spectrum shape broadens and smoothens despite the sharp step-like density of QW states. The PICS3D simulator allows to incorporate the intraband electronic relaxation model [26] into the gain spectrum $g_a(\hbar\omega)$ of a MQW laser via a convolution integral

$$g_a(\hbar\omega) = \int_{E'_g}^{\infty} g(E_{if}) L(\hbar\omega - E_{if}) \, dE_{if} \qquad (1)$$

where $g_a(\hbar\omega)$ is the material gain coefficient as a function of photon energy $\hbar\omega$, which includes the effect of the intraband relaxation, $g(E_{if})$ is the optical gain without intraband relaxation which is caused by photon-induced transitions of electrons from a conduction subband with energy E_i to a valence subband with energy E_f in the QW [27], $L(\hbar\omega - E_{if})$ is a lineshape broadening function defined by the intraband relaxation effects, $E_{if} = E_i - E_f$ is the carrier transition energy, and E'_g is the bandgap between the two subbands. A simplified version of (1) can be applied to bulk lasers if the QW subbands are replaced with the conduction and valence bands of the bulk semiconductor, respectively, and $E'_g = E_g$, the bulk material bandgap.

Several theoretical methods have been developed to approximate the lineshape function, such as in [28] (and its simplified version in [29]), where it was shown using the density operator formalism that the electron state decay with time obeys initially a Gaussian and then an exponential dependence. Other approaches give a Lorentzian lineshape, as in [30], where the scattering rate out-of-state depends on the position of the state in the band and the band filling. The PICS3D

TABLE I
STRUCTURE AND MATERIAL PARAMETERS

Symbol	Parameter Name	Value	Units
R_a	Left facet reflectivity	0.3 (z=0)	-
R_r	Right facet reflectivity	10^{-4} (z=800 μm)	-
w	TLD width	1.5	μm
L_a	Active section length	400	μm
L_{ph}	Phase section length	100	μm
L_{DBR}	DBR section length	300	μm
$d_{a,bulk}$	Bulk AR thickness	0.18	μm
$d_{a,MQW}$	Total MQW AR thickness	0.167	μm
d_p	Waveguide region thickness of phase section	0.58	μm
d_{DBR}	Waveguide region thickness of DBR section	0.38	μm
d_{gr}	Grating region thickness	0.2	μm
E_{ga}	Bandgap of bulk AR	0.7986	eV
E_{gp}	Bandgap of passive sections	0.85	eV
α_i	Average internal losses	5	cm^{-1}
κ	DBR coupling coefficient	50	cm^{-1}
A	Linear recombination	2×10^9	s^{-1}
B	Bimolecular recombination	2×10^{-10}	cm^3 s^{-1}
C	Auger recombination	7×10^{-29}	cm^6 s^{-1}

software uses a Lorentzian lineshape as a good approximation for accurate calculations of the gain spectrum in accordance with detailed discussions in [26], [27], [31]:

$$L(\hbar\omega - E_{if}) = \frac{1}{\pi} \frac{\hbar/\tau_{in}}{(\hbar\omega - E_{if})^2 + (\hbar/\tau_{in})^2}, \qquad (2)$$

where τ_{in} is the average intraband carrier relaxation time. As we will show, the gain broadening in the QW AR and, importantly, also in bulk passive sections plays a crucial role in the operation of TLDs with large wavelength tuning range. Variation of τ_{in} results in a significant change in the MQW TLD tuning and the output power performance.

In Section II the simulated TLD setup and its parameters are described in detail. In Sections III and IV the obtained simulation results for MQW and bulk TLDs are presented and discussed, respectively. Section V includes the discussion and summary of the obtained results and Section VI the conclusions.

II. DEVICE STRUCTURE AND PARAMETERS

For comparison reasons we consider two different simulation setups. The first setup is a 3-section TLD with a MQW AR operating at 1.55 μm. The AR contains 5 unstrained 7-nm thick In$_{0.56}$Ga$_{0.44}$As$_{0.94}$P$_{0.06}$ QWs and 6 unstrained 22-nm thick In$_{0.74}$Ga$_{0.26}$As$_{0.57}$P$_{0.43}$ barriers. The second setup is a TLD with a bulk In$_{0.61}$Ga$_{0.39}$As$_{0.84}$P$_{0.16}$AR also operating at 1.55 μm. The n- and p-InP cladding layers are doped at a 1×10^{18} cm^3 level. The design and material parameters are given in TABLE I.

There are two layers above and below the AR for better optical confinement. They also enhance the potential barriers and improve the injected free carrier confinement preventing possible vertical electron leakage from the AR into the p^+-region under high injection levels, as was demonstrated in [32]. The waveguide (WG) layer in all passive sections is the quaternary In$_{0.66}$Ga$_{0.34}$As$_{0.74}$P$_{0.26}$ with bandgap wavelength $\lambda_{gp} \approx 1.46\mu$m. The grating layer consists of an

$In_{0.68}Ga_{0.32}As_{0.69}P_{0.31}$ material etched into the WG quaternary. Between the WG and the p^+-region in both the DBR and the phase sections there are 6-nm thick electron stopper layers of $In_{0.53}Ga_{0.4}Al_{0.06}As$ with a bandgap wavelength $\lambda_{gb} = \lambda_{gp} \approx 1.46\ \mu m$ in order to prevent carrier leakage into the DBR p^+-region. The refractive indices of each layer and their spectral dependences on the photon energy are calculated according to the Adachi model [33]. This choice is essential since, as was demonstrated in [34], the Adachi model works especially well for photon energies close to the material bandgap, which is particularly important in tunable lasers because the passive section bandgap should be as close as possible to the lasing photon energies. The latter is necessary in order to maximise the refractive index change (thus the wavelength tuning range) under the free carrier injection [35], [36].

The device has a common bottom contact for all sections and three mutually isolated individual top contacts for each section. According to the PICS3D embodiment [16], the bottom contact should always be pre-biased in order to avoid spurious currents between the top contacts. We apply a 0.3 V pre-bias voltage in all simulated devices. The optical solver in PICS3D is switched on only at biases when the AR injection current is at or near the threshold current. Prior to this point, in order to avoid a severe convergence problem, it is required first to apply a bias current (not a voltage) to the top contact and solve the electrical problem only. Once the threshold is reached, the optical solver is switched on and the Fermi levels in the AR are clamped by large stimulated recombination. The AR current biasing continues and the coupled 3D electrical and optical problems are solved self-consistently. All investigated TLDs operated at a fixed initial (before the tuning) output power $P_0 = 3$ mW with the AR injection currents $I_a = 15 \div 18$ mA, almost double the threshold currents $I_{th} = 6 \div 9$ mA. (Note, that the threshold current I_{th} varies with tuning, as will be discussed later). The band profile of the MQW AR under 15 mA injection current is shown in Fig. 1, where $E_{c(v)}$ is the conduction (valence) band edge energy, and $E_{Fn(Fp)}$ is the electron (hole) quasi-Fermi level. The wavelength tuning is achieved by applying a forward voltage bias to the top contact of the corresponding passive section.

The parameters in TABLE 1 are similar to those used in our previous work [19] which was focused on the identification of the main physical mechanisms contributing to the electronic refractive index change and on achieving enhanced wavelength tuning of bulk TLDs. The IVBA and carrier relaxation broadening (CRB) effects had not been considered. Here the investigation concentrates on the limiting factors which define the wavelength tuning and the output power performance of bulk and MQW TLDs with similar design parameters and on the demonstration of peculiar physical effects due to the IVBA loss in passive sections of TLDs.

III. Model and Simulation Results for MQW TLD

PICS3D uses a self-consistent 3D laser model based on a drift-diffusion description of the carrier transport and traveling wave approach in describing the optical field in the cavity
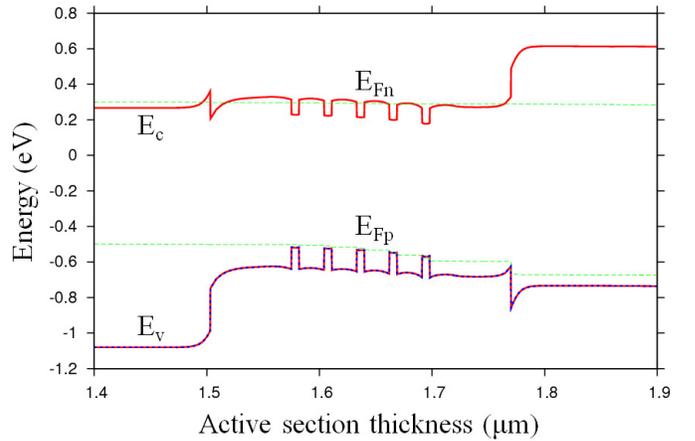
Fig. 1. Band structure profile of the MQW AR under 15 mA injection current.

by a transfer matrix formalism. The interface carrier transport at heterojunctions is described by thermionic emission model. As is seen from Fig. 1, the hole quasi-Fermi level E_{Fp} discontinuity at the right heterobarrier clearly indicates that the hole injection is actually controlled by thermionic emission. In QW lasers the carrier transport across the QW regions is described in terms of the carrier capture/escape mechanism. PICS3D utilises a phenomenological model [27] in which a fraction of thermionic emission currents at each QW/barrier interface is captured/escaped into/from the QW. The heterojunction capture/escape coefficient γ is proportional to the microscopic scattering probability between 3D and 2D states.

Different meshes are used for electrical and optical solvers. However, since simulation of a TLD requires calculation of the local refractive indices and modal gains as functions of the carrier density, these optical parameters are directly interpolated from electrical mesh at each iteration of the Newton solver. As a result of this computational approach the PICS3D simulation of TLDs is carried out in a full 3D model [16], [19].

We first investigate the case of discontinuous tuning of the MQW TLD. The electron and hole QW capture/escape parameters were defined as $\gamma_e = 0.2$ and $\gamma_h = 0.05$, respectively. The intraband relaxation time in the Lorentzian broadening function (2) was initially chosen $\tau_{in} = 1$ ps for the MQW AR and $\tau_{in} = 0.2$ ps for the bulk passive sections. (Note, that the latter value $\tau_{in} = 0.2$ ps in bulk passive sections was kept constant in all our simulations). It is important to note that the physical roles of Lorentzian broadening in the AR and in the passive sections of TLD are very different. As we will show, the main effect of the Lorentzian broadening in the passive sections is to modify the optical gain/loss there, while in the AR it increases the available wavelength tuning range and strongly affects the output power performance of the TLD.

The DBR section is tuned by applying a voltage bias to the contact V_{DBR} varied from 0 V to a maximum 2 V, which corresponds to the maximum injected DBR current $I_{DBR} \approx 400$ mA, as is seen from the I-V characteristic in Fig. 2. The DBR carrier density at this bias was $N_{DBR} \approx 5.86 \times 10^{18}$ cm^{-3}.

The phase tuning section remained unbiased during this regime. The injected carriers cause a change $\Delta n'$ of the real
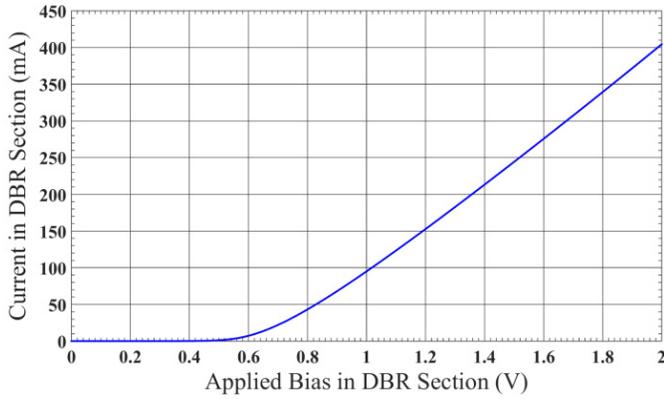
Fig. 2.   Current-voltage (I-V) characteristics of the DBR tuning section.

Fig. 4.   Band structure profile of the DBR section under 400 mA injection.

Fig. 3.   DBR wavelength tuning performance of the MQW TLD.

Fig. 5.   The output power of the MQW TLD as a function of the DBR bias.

part of the refractive index in the DBR WG region. The two main free-carrier contributions to the refractive index change in our TLD structures are the bandfilling effect and the plasma effect [35], [36]. We have shown in [19] that, contrary to usual assumption, the bandfilling effect dominates over the plasma effect at all injected carrier densities.

However, the ratio between these two contributions varies with the injection current (it increases with the current increase). For this reason it is necessary to consider both mechanisms which are included in PICS3D. The bandfilling effect is implemented via the standard Kramers-Kronig (KK) relations. Note that due to strong dispersion of the KK relations this contribution to the refractive index change also affects the spectral dependence of tuning (contrary to the weakly-dispersive plasma effect contribution). Fig. 3 demonstrates a record wavelength tuning range achieved in our TLD structure. At the maximum DBR bias we have obtained the total refractive index change equal to $\Delta n' \approx -0.086$, which results in large blue-shifted wavelength tuning between 1550 and 1518 nm over the range of $\Delta \lambda = 32$ nm. The corresponding intermode spacing is $\Delta \lambda_m \approx 0.63$ nm.

The record tuning range has been achieved using the optimised TLD design. As can easily be observed, the current injection levels to obtain this tuning range are quite high, still achievable in practical TLDs [37]. The only issue that can emerge here is the high vertical carrier leakage from the WG into the adjacent layers (especially, for the electrons), which can lead to Joule heating of the device. It was indeed found
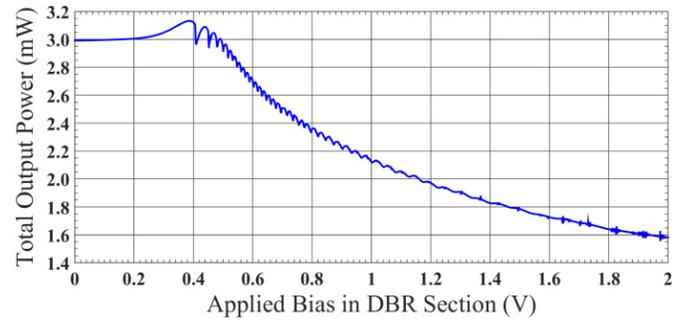
in the simulation that the (InGaAsP-WG)/(p^+-InP cladding) structure that was initially used in a non-optimised device led to leakage currents of over 73% for $V_{DBR} = 2$ V. The main reason is that this structure has a band offset ratio $\Delta E_c / \Delta E_g = 0.4$, which gives a conduction band discontinuity of only 0.2 eV (InGaAsP WG $E_g = 0.85$ eV, InP $E_g = 1.35$ eV). This discontinuity is not enough to prevent the electron spillover at high injection levels. In the optimised structure we have introduced a thin 6-nm InGaAlAs stopper layer [32] between the InGaAsP WG and the p^+-InP region which increases the potential barrier for electrons to 0.36 eV, as is shown in the band diagram of the optimised DBR section in Fig. 4. No adverse effects were observed in the TLD operation with the stopper layers as was checked in auxiliary simulations.

The InGaAlAs/InP structure has a band offset ratio $\Delta E_c / \Delta E_g = 0.72$, with InGaAlAs bandgap energy $E_g = 0.85$ eV. The result of this optimisation is a drastic drop in the leakage current to below 3% in all simulated devices, even at very high current injection levels ~400 mA.

Fig. 5 shows the output power variation with the tuning bias in the optimised TLD. As is seen, a significant drop in the output power (about 50% of the initial value) is observed at maximum tuning. As will be shown, two different physical mechanisms are responsible for the output power decrease: (i) the variation in the total optical losses in the WG passive regions during tuning; (ii) the mutual interplay between the AR net gain spectrum and the DBR mirror losses spectrum.

The total optical losses in the tuning sections have two different contributions. The first contribution is due to the tail
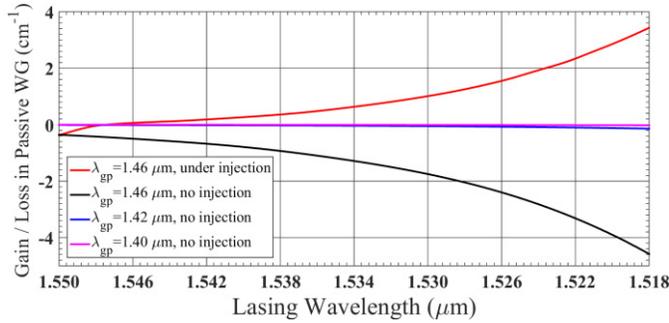
Fig. 6. Optical gain/loss spectra $g_p(\lambda)$ in the WG region of the passive sections as a function of lasing wavelength for different material bandgaps λ_{gp}.

part of the gain/absorption spectrum $g_p(\lambda)$ which extends into the bandgap region of the passive section material and enters the lasing wavelength tuning range. There are various microscopic physical models which describe the gain bandgap tails. In PICS3D only the intraband CRB model (2) is available. Fortunately, according to [20] and [37], it is the CRB model which better explains the operation of single-mode lasers, and thus its utilisation in our simulations is well-justified. The second contribution to optical losses is due to FCA and IVBA. It is important that all contributions to optical losses in the passive sections depend on the carrier density and vary with tuning. However, optical losses due to the gain bandgap tail spectrum are present even in the absence of free carriers.

During the tuning process the wavelength of the lasing mode λ_m is blue-shifted towards the WG material bandgap $\lambda_{gp} = 1.46$ μm. The WG gain/absorption in the tail region also varies with the wavelength blue-shifting. However, the resulting behaviour depends on whether the corresponding section is injected with the carriers or not. Fig. 6 shows a variation of the optical gain/loss spectrum $g_p(\lambda)$ in the passive sections with the lasing wavelength tuning for different bandgap wavelengths λ_{gp}. If any tuning section (the DBR, phase, or both) is injected, the WG optical losses in the injected section decrease with the current increase (the lasing wavelength decrease). Fig. 6 corresponds to the case when only the DBR section is injected. The non-injected phase section shows increase of the losses with tuning (black line), while in the DBR section the losses turn into gain after about 5-nm of wavelength tuning (red line).

Further increase in the DBR tuning results the gain increase in this section. In contrast, the losses in the non-injected phase section continue increasing with tuning (black line in Fig. 6). The physical reasons for such behaviour of the gain/loss in both sections are due to the carrier radiative transitions between the states in the gain tail spectral region. These transitions in a non-injected section between the filled valence subband and empty conduction subband correspond to stimulated optical absorption (loss). In the injected section the transitions between the filled conduction subband states and empty valence subband states correspond to stimulated emission (gain).

It is important to stress that the WG gain/loss becomes zero if the broadening is absent and the lineshape function is approximated by the delta-function, $L(\hbar\omega - E_{if}) \to \delta(\hbar\omega - E_{if})$,

as was directly observed in our simulations. This proves the above physical mechanism of the gain/loss in passive sections. One way to reduce this gain/loss is to select a shorter passive section bandgap wavelength λ_{gp}, so that the corresponding transition energy between the tail states increases and shifts out of the lasing range. This is demonstrated by the curves in Fig. 6 for two gap wavelengths $\lambda_{gp} = 1.42$ μm (blue line) and $\lambda_{gp} = 1.40$ μm (magenta line) when the gain/losses remain practically zero during tuning. The drawback of this approach is that the available refractive index change $\Delta n'$ in the grating region under injection also decreases with the bandgap increase, which in turn reduces the available tuning range $\Delta\lambda$. This happens because of the spectral dependence of $\Delta n'$ on the lasing wavelength, as was shown in [35] and [36]. We did observe a substantial improvement in the power output for larger WG material bandgaps, however, on expense of the tuning range reduction. For discontinuous tuning with the chosen parameters we obtained a partial mutual compensation of the phase section losses by the DBR section gain, as Fig. 6 shows.

The results in Fig. 6 are limited to the Lorentzian lineshape model. The gain/loss in passive WG region is completely defined by the electron transitions in the low-energy tail region (below the bandgap edge of the WG material). The Lorentzian model generally underestimates the gain tail magnitude in comparison with the more exact non-Lorentzian lineshape models [26], [28], and [31]. Therefore, the more advanced gain models based, for example, on many-body theory will result in a decrease of the losses (black line) and increase of the gain (red line) at the corresponding lasing wavelengths.

The second injection-dependent contribution to optical losses in the WG region is due to the FCA α_{FC} and the IVBA α_{IVBA} mechanisms. PICS3D models include both of these mechanisms. The FCA and IVBA losses are directly proportional to the injected carrier density N, and are respectively defined as $\alpha_{FC} = [e^3\lambda^2(1/m_e^2\mu_e + 1/m_h^2\mu_h)/4\pi^2c^3n\varepsilon_0]N \equiv k_{FC}N$ and $\alpha_{IVBA} = k_{IVBA}N$ [38], where $m_{e(h)}$ is the electron (hole) effective mass, $\mu_{e(h)}$ is the electron (hole) mobility, e is the electron charge, λ is the lasing wavelength, c is the speed of light in vacuum, n is the WG refractive index, ε_0 is the dielectric constant of vacuum, and k_{FC} and k_{IVBA} are the coefficients for the FCA and IVBA, respectively. Thus, the total carrier-injection-induced losses $\alpha_{ct}^{(a,p)}$ in the AR (a) or passive (p) sections can be presented as $\alpha_{ct}^{(a,p)} = k_t N^{(a,p)}$, where $k_t = k_{FC} + k_{IVBA}$ is the total free-carrier loss coefficient.

In InGaAsP lasers the IVBA contribution dominates over the FCA, but there is great uncertainty about the values of these coefficients, particularly for k_{IVBA} [17], [18], [31], [39]. In usual single-mode laser diodes the main effect of the IVBA is to increase the threshold current and to affect its temperature dependence. It was also argued that the actual impact of the IVBA effect in these lasers is rather limited [40]. As will be shown and explained here, the role of the IVBA is markedly different in TLDs because of its peculiar physical role in the passive sections in the longitudinal mode filtering by the DBR. It will be demonstrated that the IVBA contribution in the biased tuning section(s) strongly affects both the output
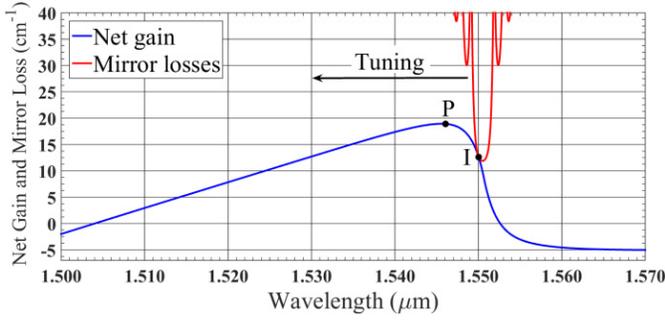
Fig. 7. Spectra of the net gain $g_{net}(\lambda)$ and the cavity mirror losses $\alpha_m(\lambda)$ of the MQW TLD at the beginning of tuning (lasing wavelength $\lambda_0 = 1.55$ μm).

power and the wavelength tuning performance of TLDs. Due to a variety of the reported FCA and IVBA parameters in various InGaAsP lasers, we consider here k_{FC} and k_{IVBA} over a realistic range of values, $k_{FC} = (0.1 \div 1) \times 10^{-18}$ cm^2 and $k_{IVBA} = (1 \div 60) \times 10^{-18}$ cm^2, for the passive sections of the TLD. Since in the AR of the TLD the FCA and the IVBA affect only the laser's threshold current and have no influence on the tuning performance of the TLD, in line with [40] we will keep the coefficients in the AR relatively small ($k_{FC} = 0.2 \times 10^{-18}$ cm^2 and $k_{IVBA} = 2 \times 10^{-18}$ cm^2) in all simulations in order to maintain a fixed AR current and power P_0.

The main difference between the FCA and IVBA losses and the internal losses (which we set here at $\alpha_i = 5$ cm^{-1}) is that they keep growing as the injection tuning current increases. The resulting influence of the FCA and IVBA losses under the TLD tuning strongly depends on the range of the DBR injection currents and the actual values of the material parameters k_{FC} and k_{IVBA}, as will be discussed later.

Another major factor which influences the TLD power behaviour shown in Fig. 5, is the mutual interplay between the net gain spectrum and the cavity mirror loss spectrum at each lasing wavelength. This is illustrated in Fig. 7 where the net gain spectrum $g_{net}(\lambda)$ of the AR at the beginning of tuning (initial lasing wavelength $\lambda_0 = 1.55$ μm) is plotted together with the mirror losses $\alpha_m(\lambda)$ spectrum of the composite cavity of length L_c created by the Bragg reflector with wavelength-selective DBR reflectivity $R_g(\lambda)$ and the left facet ($R_a = 0.3$).

The net optical gain $g_{net}(\lambda)$ in our TLD model takes into account the free carrier induced losses in all injected sections as well as gain/loss due to the CRB effect. It is calculated as

$$g_{net}(\lambda) = \Gamma_{xy}^{(a)}\frac{L_a}{L_c}\left[g_a(\lambda) - \alpha_{ct}^{(a)}\right] - \alpha_i - \sum_p \Gamma_{xy}^{(p)}\frac{L_p}{L_c}\left[\alpha_{ct}^{(p)} - g_p(\lambda)\right] \tag{3}$$

Here $g_a(\lambda)$ is the AR material gain defined in (1) which is directly calculated by PICS3D at the lasing wavelength and the threshold carrier density N_{th}, $L_c = L_a + L_{ph} + L_{eff}$ is the total composite cavity length, L_{eff} is the DBR effective length [27], and $\Gamma_{xy}^{(a,p)}$ is the transverse optical confinement factor in the MQW AR (a) and the passive WG sections (p), respectively. The last term in equation (3) describes the total losses in the
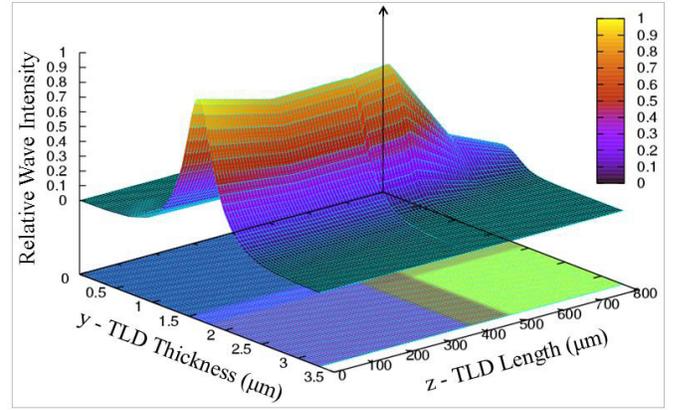
Fig. 8. Intensity distribution in the TLD for 15 mA AR injection current.

passive phase section ($L_p = L_{ph}$) and the DBR section ($L_p = L_{eff}$) due to the free carrier injection and the CRB effect, as was discussed earlier. Here we use equation (3) only for a qualitative explanation of the obtained results. PICS3D uses the 3D travelling wave model which directly calculates local 3D distributions of the optical intensity in a composite TLD cavity, as is shown in Fig. 8.

The distributions obtained in Fig. 8 allow us to estimate reasonably well the confinement factors $\Gamma_{xy}^{(a,p)}$ and the DBR effective length L_{eff}. For our TLD model we have obtained the following values: $\Gamma^{(a)} \approx 0.025$, $\Gamma^{(p)} \approx 0.8$, and $L_{eff} \approx 90.5$ μm. The carrier density which defines the material gain and the carrier-induced losses, is also calculated locally. The contribution of FC losses in the claddings is very small (for simplicity and faster convergence, they are included into the internal losses). For estimations in equation (3) we use the average value of the threshold density $N_{th} = 2.03 \times 10^{18}$ cm^{-3} in the AR. In passive sections the carrier density varies with tuning.

At lasing, the cavity gain condition is $g_{net}(\lambda) = \alpha_m(\lambda)$, where $\alpha_m(\lambda) = (1/2L_c) \ln[1/R_a R_g(\lambda)]$ is the mirror loss coefficient. As was shown in [19], the best mode selectivity in a 3-section TLD is achieved when the κL_{DBR} product of the DBR is around 1.5 (κ is the coupling coefficient, L_{DBR} is the DBR section length), which yields the maximum reflectivity $R_g(\lambda) = 0.8$ at the Bragg wavelength. The value $\kappa L_{DBR} = 1.5$ is used in all our simulations in this paper. A typical value of the mirror losses in the simulated TLDs was $\alpha_m(\lambda) \approx 12$ cm^{-1}.

In order to identify the key mechanisms of power loss under TLD tuning and their quantitative contributions, we first simulate the TLD operation for the lowest values of the carrier-induced optical loss coefficients ($k_{FC} = 0.2 \times 10^{-18}$ cm^2 and $k_{IVBA} = 2 \times 10^{-18}$ cm^2). It was found that the power loss is completely determined by the mutual interplay of the net gain and the mirror loss spectra, with all other contributions being negligibly small over the whole wavelength tuning range. This can be seen from a comparison of the curves in Fig. 9.

The blue line (which is the same as in Fig. 5) was obtained using the above optical loss coefficients, and the red line was calculated when the free carrier-induced losses were
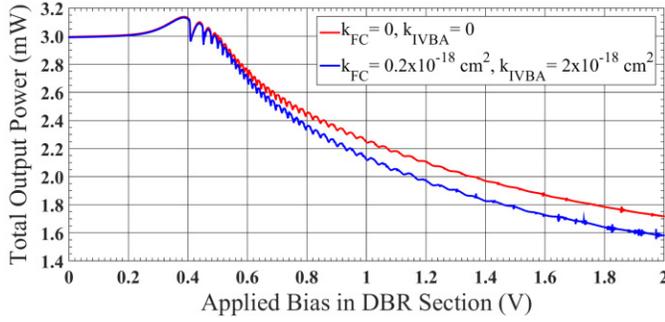
Fig. 9. The output power of the MQW TLD as a function of the DBR bias for small values of the free carrier-induced optical loss coefficients k_{FC} and k_{IVBA}.

deactivated (PICS3D allows this option). There is only a minor difference ($\sim$0.1 mW) between these results. At the very beginning of the DBR section tuning there is a small power increase from 3 mW to 3.15 mW which is due to the gain increase ($dg_{net}/d\lambda < 0$) when the wavelength is tuned in the interval between the initial wavelength $\lambda_0 = 1550$ nm and the gain peak wavelength $\lambda_p = 1547$ nm (ascending path on the net gain curve from the initial point I to the gain peak point P in Fig. 7) by increasing the DBR bias from $V_{DBR} = 0$ V to $V_{DBR} \approx 0.4$ V. (This is also in agreement with the tuning curve in Fig. 3). The increase of the net gain of the lasing mode is greater than the optical loss increase, and the output power increases. The wavelength tuning within the narrow spectral area around the gain peak point P, where the gain flattens and $dg_{net}/d\lambda \approx 0$, corresponds to a relatively small output power variation. From a practical point of view this is the best tuning and power performance regime of the TLD, but it can only be utilized within a narrow wavelength tuning range.

For a deeper blue tuning (past the gain peak point P) the net gain corresponding to the lasing mode wavelength always decreases ($dg_{net}/d\lambda > 0$). The result of the mutual positioning of the net gain spectrum and the DBR loss spectrum is to significantly decrease the output power which drops from 3 mW at the initial lasing wavelength $\lambda_0 = 1.55$ μm to 1.5 mW ($\Delta P/P \approx 50\%$) at the end for the final lasing wavelength $\lambda_{fin} = 1.518$ μm (the tuning range $\Delta\lambda \approx 32$ nm). We can conclude from this that in the regime under consideration the output power variation is mainly defined by the shape of the net gain spectrum $g_{net}(\lambda)$. In the case of a MQW AR $g_{net}(\lambda)$ strongly depends on the CRB effect and the value of the relaxation time τ_{in}. It will be shown later that the output power behaviour changes substantially with the change of the shape of the gain curve and the positioning of the mirror losses spectrum.

It is important to take into account that the output power variation in Figs. 5 and 9 does not simply follow the shape of $g_{net}(\lambda)$ spectrum. When the DBR section is tuned, the threshold current and the threshold carrier density will also vary. This in turn will result in a change of the gain spectrum. This is because the threshold net gain value is defined by the mirror loss value $\alpha_m(\lambda)$ which varies only slightly for each lasing wavelength. In the tuning region between λ_0 and λ_p the material gain increases, thus the threshold carried density must decrease in order to keep the same threshold net gain.

After reaching the gain peak wavelength λ_p, the wavelength tuning moves along the descending part of the material gain spectrum. As a consequence, the corresponding decrease of the gain results in an increase of the threshold carrier density. As a result, the net gain spectrum does not remain the same as at the beginning of the tuning (Fig. 7), but varies with tuning too.

The variation of the output power with tuning drastically changes for large values of the free-carrier-induced optical loss coefficients. Importantly, this case also allows to observe a key difference between the free-carrier-induced losses in the AR and in the passive sections of the TLD. The underlying physics behind this phenomenon can qualitatively be understood from equation (3). Typical values of the AR material gain at lasing wavelengths are $g_a(\lambda) \approx 900 \div 1000$ cm^{-1}. The values of the IVBA losses even for very large IVBA coefficients $k_{IVBA} \approx (20 \div 60) \times 10^{-18}$ cm^2 and high injection carrier densities $N_{DBR} \approx (1 \div 6) \times 10^{18}$ cm^{-3} are in the range of $\alpha_{IVBA} \approx (20 \div 360)$ cm^{-1}. Even these extreme values of the IVBA losses still remain considerably smaller than the material gain in the AR. However, the role of the IVBA losses in the passive sections is more prominent than in the AR of the TLD. This is because of considerably larger confinement factors in equation (3) in bulk passive regions in comparison with the MQW AR, $\Gamma_{xy}^{(p)}(L_p/L_c) >> \Gamma_{xy}^{(a)}(L_a/L_c)$. The clamped 3D threshold carrier density in the MQW AR $N_{th} \approx (1.5 \div 2) \times 10^{18}$ cm^{-3} in our TLD is also smaller than the maximum achievable carrier density in passive sections, $N_{DBR} \approx (5 \div 6) \times 10^{18}$ cm^{-3}. For these reasons the role of the IVBA contribution in the last term in equation (3) (passive sections) is more prominent than in the first term (AR). It increases for large IVBA coefficients and high injection tuning carrier densities and may become comparable in magnitude or larger than the mirror losses term $\alpha_m(\lambda)$. This in turn results in an unusual behaviour of the TLD with large IVBA coefficients ($k_{IVBA} > 2 \times 10^{-18}$ cm^2) under broad wavelength tuning. At small DBR biases, $V_{DBR} < 0.8$ V, when the injected carrier densities are small, the TLD operates normally, and the output power behaviour is similar to the graphs shown in Fig. 9. However, further increase of the DBR section tuning resulted in a sudden severe numerical convergence problem at some value of V_{DBR}. We think that the origin of this problem is not of computational nature, but that it reflects a real physical process in the TLD which disrupts its tuning. Further analysis of the TLD spectra supports this assertion. Fig. 10 (a) – (c) shows the evolution of the cavity comb spectra when the DBR tuning bias varies between 0.75 V and 0.85 V (the point where the convergence problem appears). These spectra were calculated for $k_{FC} = 1 \times 10^{-18}$ cm^2 and $k_{IVBA} = 10 \times 10^{-18}$ cm^2.

The cavity comb modes are calculated self-consistently for each carrier injection level in the DBR tuning section. At $V_{DBR} = 0.75$ V the TLD lases at $\lambda = 1536.6$ nm, M_1 mode in Fig. 10 (a). When the DBR bias increases from 0.75 V to 0.85 V, the Bragg wavelength is blue-shifted approaching successively the corresponding "queuing" side modes $M_2 - M_6$. Thus, there should be 6 tuned-in lasing modes. However, at $V_{DBR} = 0.8$ V the comb mode M_6 is missing,
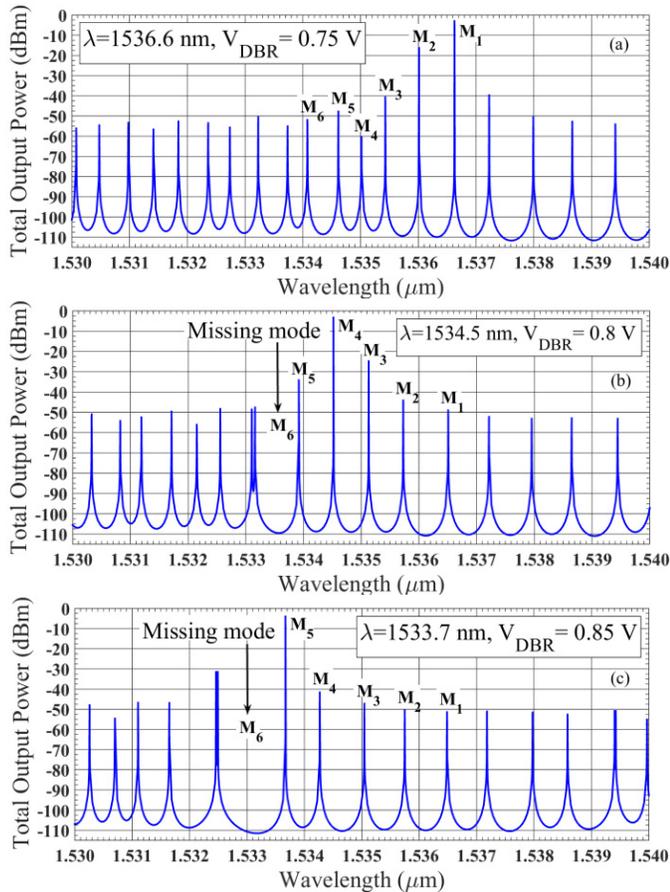
Fig. 10.   Evolution of the TLD cavity comb mode spectrum with the DBR section tuning. The modes labeled as $M_1 – M_6$ are the modes that become the lasing modes under the tuning. The lasing mode has the highest power.

Fig. 11.   Lasing spectrum obtained in the VPI simulation showing the lasing mode M_6 at $V_{DBR} = 0.92$ V which was missing in the PICS3D simulation.
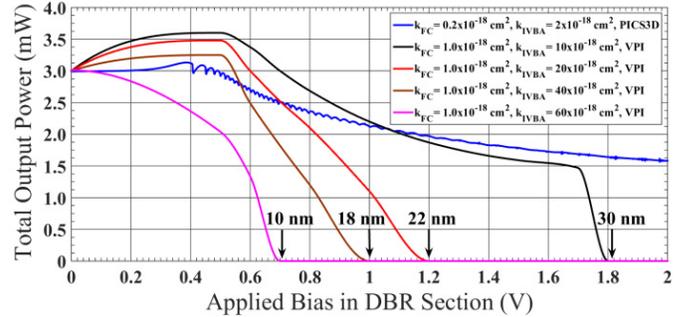
Fig. 12.   The output power of the MQW TLD as a function of the DBR bias for small and large values of the free-carrier-induced optical loss coefficients.

as is seen in Fig. 10 (b). The physical reason for this is the high IVBA losses in the DBR section. Due to these high losses the DBR ceases to function efficiently as a cavity mode selector. At $V_{DBR} = 0.85$ V the comb mode M_5 becomes the lasing mode, shown in Fig. 10(c). Further tuning of the DBR section shifts the Bragg wavelength towards mode M_6 which would become the lasing mode if it would be present, while lasing mode M_5 moves out of the DBR stopband. As a result, the M_5 mode stops lasing due to high mirror losses outside of the DBR stopband, and mode M_6 is not turned on as it is missing. The TLD ceases lasing altogether at $V_{DBR} > 0.85$ V. In accordance with the PICS3D numerical procedure, the absence of the cavity comb mode means that the optical solver is unable to simulate lasing and this is manifested as a non-convergence problem.

The assumption that IVBA losses in the tuning sections are responsible for poor DBR mode selectivity has also been supported by an auxiliary PICS3D simulation of the same TLDs but with the introduction of a small reflection ($\leq$0.1) at the DBR facet. We found that this increases the backward reflected wave power and improves the DBR mode selectivity. The TLD tuning was extended by a few more nanometers beyond the non-convergence point until it failed again due to missing modes at higher DBR tuning currents. This may be seen as an improvement of the TLD tuning performance,

however, introducing an additional facet reflection drastically decreases the SMSR, and thus is not practically useful.

Because of the practical importance of the observation about the missing cavity modes due to IVBA losses in the tuning sections for the real-world multi-section laser devices, we have carried out an additional simulation of the output power variation under the TLD tuning using the VPI software [41]. VPI is a simplified 1D solver which first solves for the comb modes in a cold cavity ignoring the losses. The obtained set of the cavity modes is maintained during tuning, thus there is no missing mode problem. We have calibrated the VPI and PICS3D models of the TLD using the recently developed integrated model [42], so both models show similar tuning and power performance of the TLD. The integrated model exports the PICS3D-calculated gain spectra into VPI by using a special interface facility available in the recent version of VPI [41].

The (filtered) lasing spectrum obtained in the VPI simulation for $k_{FC} = 1 \times 10^{-18}$ cm^2 and $k_{IVBA} = 10 \times 10^{-18}$ cm^2 at the DBR bias $V_{DBR} = 0.92$ V (above the point $V_{DBR} = 0.8$ V where the PICS3D simulations do not converge) is shown in Fig. 11. The M_6 cavity comb mode is clearly present, and it is lasing.

The results of the output power simulations are shown in Fig. 12. For small loss coefficients, $k_{FC} = 0.2 \times 10^{-18}$ cm^2 and $k_{IVBA} = 2 \times 10^{-18}$ cm^2, both the PICS3D and the VPI results are reasonably close to each other. (For bulk TLDs the curves practically coincide, as will be shown in Section IV). For large IVBA loss coefficients VPI was capable to overcome the PICS3D convergence problem and complete the simulation.

The main goal of the carried analysis was to get insight into what is happening in the TLD with large values of the IVBA
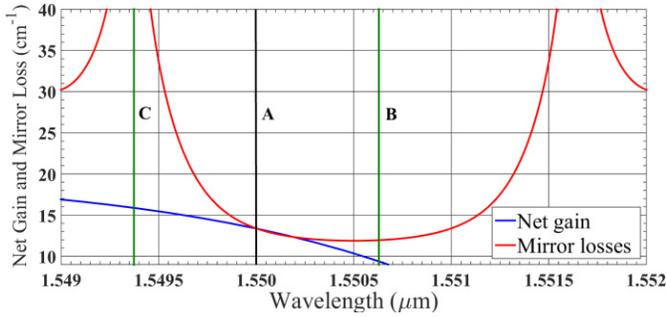
Fig. 13. Mutual positioning of the cavity modes (lines A, B, C) with respect to the mirror loss $\alpha_m(\lambda)$ (red line) and net gain $g_{net}(\lambda)$ (blue line) spectra of the MQW TLD at the beginning of tuning (lasing wavelength $\lambda_0 = 1.55$ μm).

Fig. 14. Spectra of the net gain $g_{net}(\lambda)$ and the cavity mirror losses $\alpha_m(\lambda)$ of the MQW TLD lasing at $\lambda_0 \approx 1.548$ μm for the CRB parameter $\tau_{in} = 1$ ps. The insert shows the TLD emission spectrum with the lasing mode marked by I. The labels of the axes in the insert are the same as in Fig. 10.

loss coefficients at the DBR biases when the PICS3D simulation does not converge. This takes place at the points which approximately correspond to the beginning of a steep decrease of the output power for each VPI curve shown in Fig. 12.

The larger is the IVBA coefficient k_{IVBA} the smaller is the corresponding V_{DBR} bias (and smaller is the corresponding injected carrier density) for the onset of a steep fall of the output power. More importantly, the steep decrease of the output power with the DBR tuning bias limits the achievable wavelength tuning range $\Delta\lambda$ (it is marked by the vertical arrows with the corresponding value for each curve in Fig. 12). For example, the tuning range drops from $\Delta\lambda = 32$ nm to $\Delta\lambda = 10$ nm when k_{IVBA} increases from 2×10^{-18} cm^2 (blue line) to 60×10^{-18} cm^2 (magenta line).

We also found that increasing the AR current even further in order to maintain the same initial output power does not change this behavior substantially. It is very likely that the strong impact of the IVBA losses on the mode selectivity in the DBR section is the main reason in real TLD devices which limits their power and wavelength tuning performance.

As an additional confirmation of the different roles played by the IVBA losses in the AR and passive sections of the TLD, we have simulated an extreme case of very large values of the IVBA losses, $k_{IVBA} = (100 \div 200) \times 10^{-18}$ cm^2, in the AR, but keeping it small, $k_{IVBA} = 2 \times 10^{-18}$ cm^2, in the passive sections. We found that except for a considerable increase in the AR pumping current in order to maintain the same initial output power $P_0 = 3$ mW (due to the increase of the threshold current because of large AR IVBA losses), there was no other impact on the TLD power performance under the DBR tuning.

Apart from the overall power variation, there are also numerous repeating oscillations of the output power taking place in the process of wavelength tuning, as shown in Fig. 9 and Fig. 12 (blue line). Similar oscillations of power and side mode suppression ratio (SMSR) were also observed in [11] and [12]. These oscillations can be explained by observing the mutual positioning of the cavity modes with respect to the mirror loss spectrum $\alpha_m(\lambda)$ and the net gain spectrum $g_{net}(\lambda)$, and its variation during the DBR tuning, as is shown in Fig. 13.

At the beginning of tuning the lasing mode $\lambda_0 = 1.55$ μm corresponds to line A in Fig. 13 (with a zero cavity gain). Under tuning the DBR mirror reflectivity spectrum $\alpha_m(\lambda)$ is blue-shifted toward the next comb mode indicated by line C.
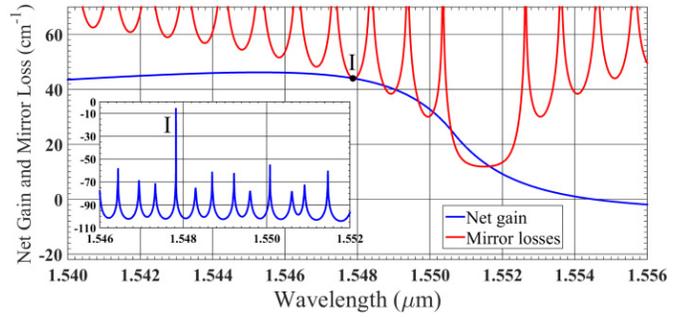
The mirror loss will slightly decrease as it approaches the bottom of $\alpha_m(\lambda)$ (this variation of $\alpha_m(\lambda)$ corresponds to the interval between lines A and B). The stationary lasing mode λ_0 at A experiences a decrease of the mirror losss and the output power increases reaching its maximum. Further DBR tuning results in a slight increase of the mirror loss and the output power decreases. After the DBR spectrum (Bragg wavelength) is tuned by the amount equal to the intermode spacing $\Delta\lambda_m \approx 0.63$ nm, the lasing mode at A jumps to a new lasing comb mode at C and the process is repeated.

Having described the power behaviour of the TLD in Fig. 12, we can also consider how to optimise the TLD performance. As is seen from Figs. 9 and 12, a significant power decrease starts almost at the beginning of tuning at $V_{DBR} \approx 0.5$ V. The main reason why the power drops so early during tuning is the proximity of the initial lasing wavelength to the gain peak, as is shown in Fig. 7. Therefore, in order to delay the power reduction so that it starts later at shorter wavelengths in the tuning range, it would be desirable to red-shift the initial lasing wavelength λ_0 by increasing the Bragg wavelength of the DBR section. In this case the ascending part of the $g_{net}(\lambda)$ curve will be wider during tuning and the power loss will start at shorter wavelngths compared to Fig. 12. For example, in our case a reasonable positive net gain can be obtained at $\lambda_0 = 1.553$ μm without a significant increase of the threshold current. It turned out, however, that in MQW TLDs this design option strongly depends on the CRB parameter τ_{in}. The physical reason for this effect is quite subtle. Using in AR $\tau_{in} = 1$ ps (the same as in all previous simulations) and designing the DBR with the Bragg wavelength red-shifted towards 1.552 μm, we found that contrary to the expectations, the initial lasing wavelength was actually not red-shifted, but blue-shifted to $\lambda_0 \approx 1.548$ μm. This occurs because of a peculiar mutual positioning of the net gain spectrum $g_{net}(\lambda)$ and the cavity mirror loss spectrum $\alpha_m(\lambda)$ in the TLD with a MQW AR. Fig. 14 shows the $g_{net}(\lambda)$ (blue line) and $\alpha_m(\lambda)$ (red line) spectra of the TLD obtained for the AR threshold carrier density $N_{th} = 2.13 \times 10^{18}$ cm^{-3}.

A careful analysis of Fig. 14 shows that although the mirror losses $\alpha_m(\lambda)$ within the DBR stopband are smaller than the losses within the next three blue-shifted sidebands, the net gain is also smaller within the main stopband. The mode inside of the $\alpha_m(\lambda)$ sideband at $\lambda \approx 1.548$ μm has a greater g_{net} value
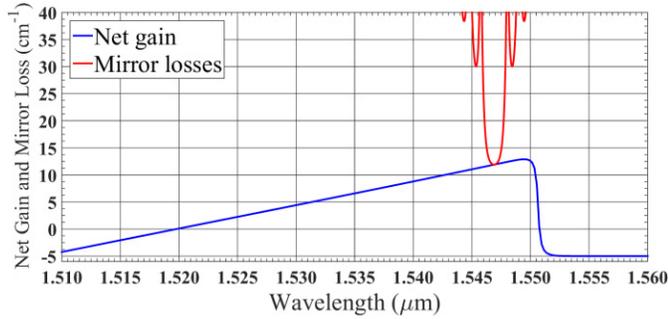
Fig. 15. Spectra of the net gain $g_{net}(\lambda)$ and the cavity mirror losses $\alpha_m(\lambda)$ of the MQW TLD lasing at $\lambda_0 = 1.547$ μm for the CRB parameter $\tau_{in} = 10$ ps.

Fig. 16. Spectra of the net gain $g_{net}(\lambda)$ and the cavity mirror losses $\alpha_m(\lambda)$ of the MQW TLD lasing at $\lambda_0 = 1.556$ μm for the CRB parameter $\tau_{in} = 0.1$ ps.

than the mode at the centre of the main stopband at $\lambda \approx 1.551$ μm. Therefore, conditions for lasing are more favourable for mode I inside the DBR sideband and it wins the lasing mode competition. This is also indicated in Fig. 14 by a zero cavity gain for this mode (point I). The main physical reason for this peculiar situation is the property of the QW gain spectrum which has a steep ascending part due to a step-like behaviour of the energy dependence of the 2D density of states. Such situation is not possible in TLDs with a bulk AR.

To further support this argument, we have simulated with PICS3D the 'ideal' case of a TLD with exactly the same parameters as were used in Fig. 9, $k_{FC} = 0.2 \times 10^{-18}$ cm^2 and $k_{IVBA} = 2 \times 10^{-18}$ cm^2 (blue curve), but with a practically unbroadened gain spectrum which is obtained for a large CRB parameter $\tau_{in} = 10$ ps in the Lorentzian lineshape broadening function. (Large carrier scattering times $\tau_{in} \geq 10$ ps yield a gain spectrum identical to the unbroadened one with a very steep ascending part [43]). It was found that it is impossible to achieve the TLD lasing at any initial wavelength located within the ascending part of the gain spectrum curve $g_{net}(\lambda)$ due to the extreme narrowness of the ascending part (~ 1 nm). This will strongly affect the output power behaviour with tuning. The corresponding spectra of the net gain $g_{net}(\lambda)$ and the mirror loss $\alpha_m(\lambda)$ in the TLD with $\tau_{in} = 10$ ps are shown in Fig. 15. The threshold 3D carrier density in the MQW AR was $N_{th} = 1.85 \times 10^{18}$ cm^{-3}.

Here the only spectral region where lasing can actually take place is at the descending part of the gain curve. For the case shown in Fig. 15, the initial lasing wavelength is $\lambda_0 = 1.547$ μm. Because such a MQW TLD will operate at the discending part of the net gain spectrum $g_{net}(\lambda)$, it is easy to conclude that the output power decrease will immediately occur from the very beginning of the DBR tuning (see Fig. 17 later).

In order to complete the investigation of how the CRB affects the tuning and power performance of the MQW TLD, we consider the case of an extreme lineshape broadening which is obtained for a small EBR parameter $\tau_{in} = 0.1$ ps in the Lorentzian lineshape function. The corresponding net gain $g_{net}(\lambda)$ and mirror loss $\alpha_m(\lambda)$ spectra of the TLD obtained at $N_{th} = 2.21 \times 10^{18}$ cm^{-3} are shown in Fig. 16.

As is seen, the ascending part of the net gain spectrum $g_{net}(\lambda)$ becomes considerably wider and the Bragg wavelength can be red-shifted as much as 6 nm so that the initial lasing wavelength is $\lambda_0 = 1.556$ μm. The CRB effect on the
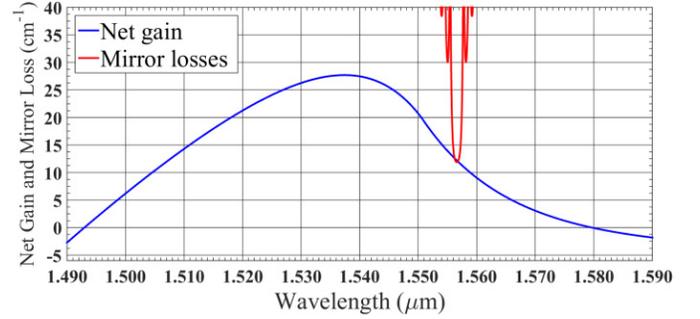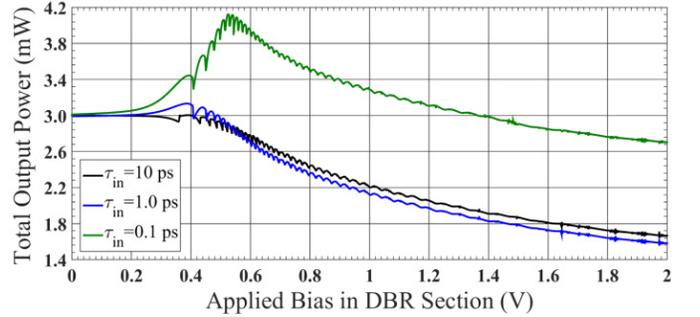
Fig. 17. Effect of the gain lineshape broadening on the output power of the DBR-tuned MQW TLD with different CRB parameters: $\tau_{in} = 10$ ps (black line), $\tau_{in} = 1$ ps (blue line), and $\tau_{in} = 0.1$ ps (green line).

gain spectrum also results in an improvement of the output power performance of the TLD under DBR tuning. Fig. 17 shows the effect of the CRB parameter τ_{in} on the output power.

A non-monotonous behaviour of the output power versus the DBR bias with about a 30% increase at the beginning of tuning for a large gain broadening (green line) can be understood with the help of Fig. 16, which indicates a wide ascending part of the gain spectra where the power increases with tuning simply due to the gain increase. In general, the broadening of the gain spectra improves the power performance of the MQW TLD.

The overal results obtained in this section demonstrate the existence of rich design options in multi-section MQW TLDs depending on desirable performance characteristics, particularly the lasing wavelength, the wavelength tuning range, and the output power variation with tuning. However, these design options strongly depend on the physical parameters of the laser structure, such as the IVBA coefficients k_{IVBA} in the tuning sections and the lineshape CRB parameter τ_{in} in the active gain section of the TLD. This in turn necessitates a careful evaluation of these parameters in each laser structure prior to the TLD design and its performance optimisation.

IV. SIMULATION RESULTS FOR BULK TLD

In order to evaluate and compare the effect of the limiting factors which were investigated in the previous section on the performance of MQW and bulk TLDs, we have carried out the simulation of a TLD with a bulk In$_{0.61}$Ga$_{0.39}$As$_{0.84}$P$_{0.16}$ AR. It has exactly the same parameters as the MQW TLD in Fig. 1 with a bandgap wavelength of the bulk AR $\lambda_g = 1.553$ μm,
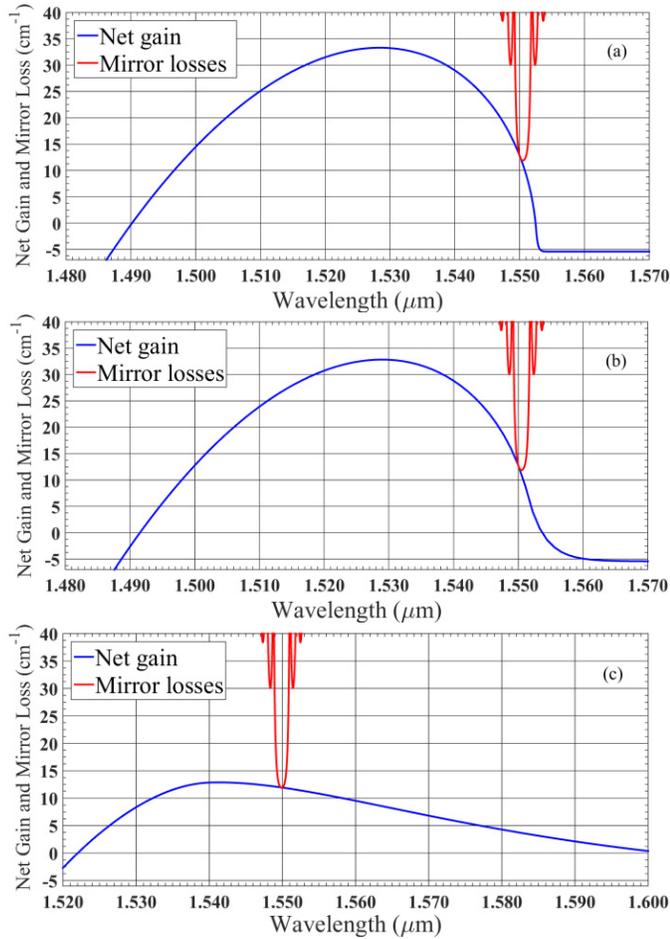
Fig. 18. Spectra of the net gain $g_{net}(\lambda)$ and the cavity mirror losses $\alpha_m(\lambda)$ of the bulk TLD lasing at $\lambda_0 = 1.550$ μm for different values of the CRB parameter: (a) $\tau_{in} = 10$ ps, (b) $\tau_{in} = 1$ ps, and (c) $\tau_{in} = 0.1$ ps.

and it operates at the same initial lasing wavelength $\lambda_0 = 1.55$ μm and output power $P_0 = 3$ mW (with AR injection currents $I_a = 11 \div 15$ mA, almost double the threshold currents $I_{th} = 5 \div 7$ mA). The DBR wavelength tuning of the bulk TLD produces a similar dependence as is shown in Fig. 3 (for more details about the tuning of the bulk TLD see [19]). We first assume small values of FCA and IVBA coefficients in all sections of the TLD ($k_{FC} = 0.2 \times 10^{-18}$ cm^2 and $k_{IVBA} = 2 \times 10^{-18}$ cm^2).

The investigation of the CRB effect in bulk TLDs has produced exactly the opposite results than the results for MQW TLDs in terms of power performance for the corresponding values of τ_{in}. This is because of the smooth ascending part of the $g_{net}(\lambda)$ spectrum in the bulk AR even in the absence of lineshape broadening. The corresponding spectra of $g_{net}(\lambda)$ and $\alpha_m(\lambda)$ at the beginning of tuning ($\lambda_0 = 1.55$ μm) are shown in Fig. 18 for different CRB parameters: (a) $\tau_{in} = 10$ ps, (b) $\tau_{in} = 1$ ps, and (c) $\tau_{in} = 0.1$ ps. The corresponding threshold carrier densities are: (a) $N_{th} = 1.13 \times 10^{18}$cm^{-3}, (b) $N_{th} = 1.12 \times 10^{18}$cm^{-3}, and (c) $N_{th} = 0.92 \times 10^{18}$ cm^{-3}.

The gain spectrum shown in Fig. 18 (a) for $\tau_{in} = 10$ ps corresponds to a practically unbroadened bulk material spectrum. Due to smooth energy dependence of 3D density of states near the bandgap energy this spectrum has relatively smooth
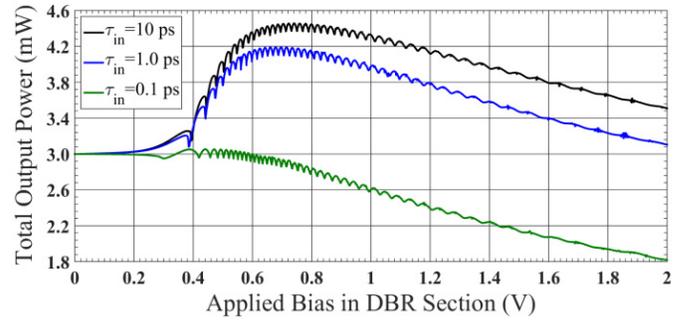
Fig. 19. Effect of the gain lineshape broadening on the output power of the DBR-tuned TLD with a bulk AR with different CRB parameters: $\tau_{in} = 10$ ps (black line), $\tau_{in} = 1$ ps (blue line), and $\tau_{in} = 0.1$ ps (green line).

ascending part in comparison with the corresponding MQW case shown in Fig. 15. In the other limit of large broadening shown in Fig. 18 (c) for $\tau_{in} = 0.1$ ps, the 3D gain spectrum becomes almost flat, which is also very different from the MQW case in Fig. 16. As a result, when the bulk TLD is DBR-tuned, its output power behaviour is strikingly different in comparison with the MQW TLD for the same CRB parameters.

The effect of the lineshape broadening on the output power in the bulk TLD under DBR tuning is shown in Fig. 19.

As is seen, the output power substantially drops (to about 60% of its initial value) with the DBR tuning in the case of a small CRB parameter, $\tau_{in} = 0.1$ ps. For larger CRB values, $\tau_{in} = 1 \div 10$ ps, the power varies non-monotonically, and it never drops below its initial value $P_0 = 3$ mW for the whole DBR tuning range. The output power can be kept constant at the initial value $P_0 = 3$ mW by the required change in the AR pumping current. However, this is easier to achieve in the case of a large value of the CRB parameter τ_{in} which will require decreasing the initial AR pumping current, while for small τ_{in} the active current may require a substantial increase. On the other hand, the gain spectra for small values of the CRB parameter τ_{in} are substantially broadened towards the red-shifted wavelengths away from the bandgap wavelength, as can be seen from Fig. 18 (c). This in turn allows to expand the range of the lasing wavelengths available for tuning by red-shifting the initial Bragg wavelength, another important option for the TLD design optimisation.

The CRB effect in bulk and MQW TLDs was simulated using the Lorentzian lineshape model. The use of the more exact non-Lorentzian lineshapes will not change the overall behaviour of the output power with the variation of the CRB parameter τ_{in}. This is because all lineshape models have a similar feature – smaller CRB parameter τ_{in} results in bigger gain spectrum broadening. The results shown in Figs. 17 and 19 are defined by the shape of the gain spectrum in the active region (unlike the results in Fig. 6, which are defined by the gain/loss spectra in the passive regions). Although, the non-Lorentzian lineshape will affect the gain shape too, however, the biggest influence will be on the threshold current, which is not essential for the results in question.

The effect of the FCA and IVBA losses on the bulk TLD performance is shown in Fig. 20 for the same set of
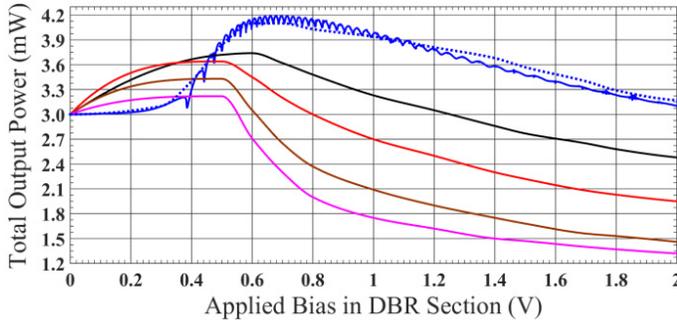
Fig. 20. The output power of the bulk TLD as a function of the DBR bias for various values of the free-carrier-induced optical loss coefficients. The colour coding of all lines is the same as in Fig. 12. The blue solid line was obtained from PICS3D and the blue dotted line is the result of the VPI simulation.

Fig. 21. Quasi-continuous wavelength tuning of the MQW and bulk TLDs for two different phase section lengths: $L_{ph} = 100$ μm and $L_{ph} = 300$ μm.

Fig. 22. Quasi-continuous wavelength tuning of the MQW and bulk TLDs with $L_{ph} = 100$ μm over the whole tuning range of $\Delta\lambda = 32$ nm.

the loss coefficients k_{FC} and k_{IVBA} as for the MQW TLD in Fig. 12. The CRB parameter in this case was kept constant at $\tau_{in} = 1$ ps. Because in both the MQW and bulk TLDs the tuning sections have exactly the same parameters and design, the output power behaviour has similar trends.

For large values of the k_{FC} and k_{IVBA} coefficients there was a severe convergence problem of the PICS3D simulation at higher DBR biases, and we had to use the VPI simulator integrated with PICS3D in order to complete the simulation. (Observe a very good quantitative agreement between the PICS3D and the VPI results in Fig. 20 for small k_{FC} and k_{IVBA}, the blue solid and dotted lines, respectively (although, the VPI does not pick up fine power oscillations). This indicates a good calibration of both TLD models). The physical reason for such behaviour is due to missing comb modes because of poor mode selectivity of the DBR section at a high IVBA loss. The fact that the output power does not drop to zero for the VPI simulated devices (as it was in the case of the MQW TLDs shown in Fig. 12) indicates that the tuning performance of the bulk TLDs is more robust than that of the MQW TLDs due to a larger net gain in the tuning wavelength interval, as can be seen from the comparison of $g_{net}(\lambda)$ in Fig. 18 (b) and Fig. 7.

Finally, we investigate the performance of the MQW and bulk TLDs under quasi-continuous wavelength tuning. For simplicity we consider the case of small k_{FC} and k_{IVBA} loss coefficients in order to avoid a convergence problem. Starting from the initial lasing wavelength $\lambda_0 = 1.55$ μm, the DBR and phase sections have been driven simultaneously with a careful selection of the applied biases.

The phase section was driven to a maximum applied bias of $V_p = 1.8$ V which corresponds to the injection current $I_p \approx 125$ mA and the carrier density $N_p \approx 5.3 \times 10^{18}$cm^{-3}. The DBR section was driven to a maximum bias of $V_{DBR} = 0.6$ V with $I_{DBR} \approx 3.9$ mA and $N_{DBR} \approx 0.7 \times 10^{18}$ cm^{-3}. The achieved continuous wavelength tuning as a function of the phase section bias was 5.7 nm, as is shown in Fig. 21. The wavelength was continuously tuned over the range of 5.7 nm from $\lambda_0 = 1550$ nm (at $V_p = 0$ V, $V_{DBR} = 0$ V) to $\lambda_f = 1544.3$ nm (at $V_p = 1.8$ V, $V_{DBR} = 0.6$ V). In order to limit a possible leakage current in the phase section, the same InGaAlAs blocking layer between the WG and the p^+ region of the phase section was introduced, as in the DBR section.
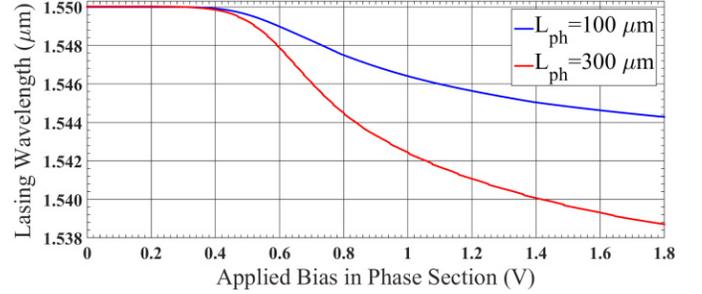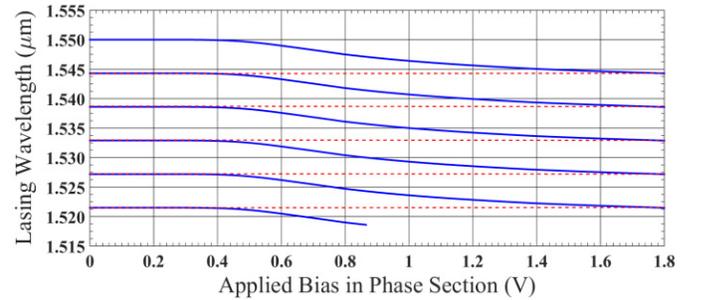
It is physically interesting and important from a practical point of view that the quasi-continuous wavelength tuning of a TLD can be substantially increased by simply designing a longer phase section L_{ph}. For example, for $L_{ph} = 300$ μm the achieved quasi-continuous tuning wavelength range becomes 11 nm, as is seen from Fig. 21, red line. Although an increase of L_{ph} results in a decrease of the intermode spacing from $\Delta\lambda_m \approx 0.63$ nm to $\Delta\lambda_m \approx 0.47$ nm, the main reason for the increase of the quasi-continuous wavelength tuning range is because of increase of the optical wave path in the longer phase section.

The obtained quasi-continuous tuning shown in Fig. 21, can still be further extended towards the shorter wavelength. This is achieved by de-biasing the phase section back to $V_p = 0$ V and carefully biasing the DBR section to the nearest lasing mode in the vicinity of the final wavelength $\lambda_f = 1544.3$ nm. Note, that this may produce a small jump away from the final lasing wavelength which is less than the intermode spacing $\Delta\lambda_m \approx 0.63$ nm in our TLDs. After this, both sections are again biased simultaneously with a careful selection of both biases. This process is repeated again until the maximum allowed bias of the DBR section is achieved. This regime of quasi-continuous tuning is shown in Fig. 22 for a TLD with $L_{ph} = 100$ μm.

The maximum quasi-continuous wavelength tuning range is limited by the maximum achievable carrier density in the phase section [38]. This in turn can be defined by the values of the free-carrier loss coefficients k_{FC} and k_{IVBA}, as was discussed earlier for the DBR section. The physical analysis which we have carried out for the DBR section regarding the effect of the IVBA and the CRB parameters, is applicable to the
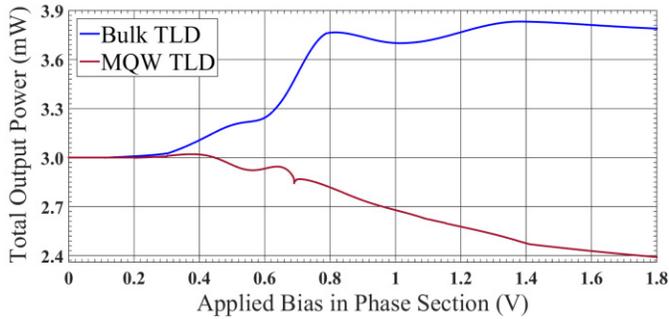
Fig. 23. The output power of the MQW and bulk TLDs with $L_{ph} = 100$ μm as a function of the phase section bias under quasi-continuous tuning.

phase section too. It is therefore crucial that before designing a real TLD one must first investigate these parameters in the real laser structure. In spite of the similar quasi-continuous wavelength tuning performance of the MQW and bulk TLDs shown in Fig. 21, their power performances are very different.

The output power versus the phase section bias for the MQW and bulk TLDs with $L_{ph} = 100$ μm is shown in Fig. 23. The main reason which is responsible for the different behaviour of the output power in the MQW and bulk TLDs under quasi-continuous tuning is the difference in the shapes of the net gain spectra near the lasing wavelength, as can be seen from the comparison of Fig. 7 and Fig. 18 (b). The power response mainly follows the net gain spectrum shape with some additional features which reflect the fact that both sections are now biased and a complex balance of gain and absorption in the composite TLD cavity takes place due to physical mechanisms which were discussed in detail in this and the previous sections. Extending the quasi-continuous tuning to yet shorter wavelengths will lead to the output power decrease in both the MQW and bulk TLDs, as can be understood from Figs. 16 and 18. Nevertheless, a careful analysis of the lasing wavelength and the output power behaviour with tuning, similar to the ones shown in Figs. 21 and 23, allows to design real TLDs with the best optimised performance in terms of accessible wavelengths and power stability, using laser structures with known CRB and IVBA physical parameters.

V. DISCUSSION OF THE RESULTS

An advanced physics-based simulation model of three-section InGaAsP/InP TLDs with MQW and bulk ARs has been developed in order to investigate their wavelength and output power performance under various wavelength tuning regimes. The key result of our simulations is the finding of a new effect in TLDs which is responsible for the collapse of the spectral mode selectivity by the DBR due to large IVBA losses in the passive phase and DBR sections. The model is based on the travelling wave formalism and is implemented using the commercial laser simulation software tools PICS3D and VPI, including their mutual calibration and integration. We found that the two parameters of the laser structure which play a crucial role in the tuning operation of the TLDs are the IVBA loss coefficient k_{IVBA} in the passive sections of the

device, and the CRB parameter τ_{in} of the Lorentzian lineshape function in the active and passive sections.

The TLD wavelength tuning and output power performance is also strongly affected by the shape of the AR net gain $g_{net}(\lambda)$ and mirror loss $\alpha_m(\lambda)$ spectra and their mutual positioning with respect to the lasing cavity mode during the tuning. The latter effect is particularly important in TLDs with a wide wavelength tuning range [3], [19], it does not directly depend on the magnitude of the k_{IVBA} coefficient, but is sensitive to the values of the CRB parameter τ_{in}.

It is demonstrated that the role of the IVBA and CRB parameters in the TLDs is very different from their role in conventional fixed-wavelength lasers. In the latter case the main effect of both parameters is to change the laser threshold current (at least in the CW regime): the CRB modifies the gain spectrum and the IVBA directly contributes to the cavity losses which are proportional to the AR injected carrier density, $\alpha_{IVBA} = k_{IVBA}N_{AR}$. In the case of TLDs, the IVBA mechanism has a strong influence on both the output power variation and the lasing wavelength tuning under the passive section biasing. Importantly, the IVBA contribution to the TLD's performance in passive and active sections is very different. The role of the IVBA losses in the AR of TLDs is quite similar to its role in fixed-wavelength lasers – just to increase the threshold current, and, in agreement with [17], it has only a slight effect even for large values of k_{IVBA} coefficients because at the clamped carrier density the IVBA losses are always smaller than the material gain. In passive sections the IVBA losses $\alpha_{IVBA} = k_{IVBA}N_p$ may become comparable to the mirror losses if the IVBA coefficient k_{IVBA} is large and/or the injected carrier density N_p is high. As a result, the DBR section ceases to function efficiently as a cavity lasing mode selector due to missing comb modes under the wavelength tuning. The output power drops sharply and the wavelength tuning operation of the TLD is disrupted. For example, the simulated TLDs with small IVBA passive section coefficients, $k_{IVBA} \leq 2 \times 10^{-18}$ cm^2, demonstrated a record wide wavelength tuning range of 32 nm. For large passive section IVBA coefficients, $k_{IVBA} \geq 60 \times 10^{-18}$ cm^2, the available tuning wavelength was less than 10 nm. Practically the same wavelength tuning behaviour has been observed in TLDs with MQW and bulk ARs. At the same time, even extremely large IVBA coefficients, $k_{IVBA} \geq 100 \times 10^{-18}$ cm^2, in the AR of the TLD do not produce any dramatic effect, except increasing the threshold current. We assert that a drastic decrease in the cavity mode selection efficiency of the injected DBR section due to the IVBA losses is the actual mechanism in real TLDs which is responsible for limiting the available wavelength tuning range in spite of the continuing refractive index change. The usual assumption that the maximum tunability is defined by the maximum achievable refractive index change [3], [38], is only correct if the IVBA loss in passive sections is small.

The output power behaviour under the TLD tuning strongly depends on the CRB parameter τ_{in}, as well as on the design of the AR (MQW or bulk). Again, there is a qualitative difference between the CRB effect in the AR and in the passive sections. Because the material bandgap in passive sections is greater than in the AR, in an ideal case (with no CRB

effect included) there would be no interband absorption of the lasing light in the passive sections. The inclusion of CRB in the passive sections results in that the long-wavelength tail of the gain/absorption spectrum $g_p(\lambda)$ extends into the bandgap region of the passive section material entering the lasing wavelength range. As a result, in non-injected passive section(s) there is an additional absorption due to the upward interband transitions between the states in the tail part of the gain/absorption spectrum $g_p(\lambda)$. If the passive section is injected with carriers, the downward stimulated interband transitions between the tail states provide some additional gain at the lasing wavelength. Such behaviour of $g_p(\lambda)$ in passive sections affects the output power.

The gain/loss contributions to the output power variation due to the CRB effect in the passive sections are not as important as the CRB contribution in the AR. In addition, the CRB effect has a different impact on the power performance of TLDs with MQW and bulk ARs because of the different shapes of the net gain spectra $g_{net}(\lambda)$ in these cases. We demonstrate that in the TLDs with a MQW AR the output power changes non-monotonically with tuning for a small CRB parameter $\tau_{in} = 0.1$ ps and it remains above its initial value $P_0 = 3$ mW for most of the wavelength tuning range. For larger values, $\tau_{in} > 1$ ps, the power monotonically decreases with tuning, and it drops about 50% at the end of tuning. The effect of τ_{in} is precisely opposite in the TLDs with a bulk AR. This behaviour is similar for both discontinuous and quasi-continuous wavelength tuning regimes. At the same time, a small τ_{in} allows to expand the available wavelength tuning range in both the MQW and bulk TLDs.

In widely tunable TLDs the strongest effect on the output power performance is, however, due to the shapes of the AR net gain $g_{net}(\lambda)$ and the cavity mirror loss $\alpha_m(\lambda)$ spectra and their mutual positioning with respect to the lasing cavity mode during tuning. Although, in the present paper we have demonstrated this point for a 3-section laser, the effect in question is universal and should be observed in TLDs with various designs of tuning sections [44]–[50]. For example, the 40-nm tuning range in both C- and L-band digital supermode DBR (DS-DBR) TLDs has been reported in [44] and [45], and the output power drop was about 30% when the laser is continuously tuned over each supermode (~7 nm). The power drop has been explained by the spectral variation of the IVBA and Auger recombination losses in the AR. Taking into account the small values of all injected tuning currents (below 70 mA) and the small continuous tuning range, we believe that the actual reason for the power variation is the variation with tuning of the mutual positioning of the net gain and the DBR reflectivity relative to the lasing longitudinal cavity mode. It is likely that the same mechanism was behind the power variation in sampled-grating DBR (SG-DBR) TLDs reported in [3] and [46]. A huge output power decrease from 22 to 7 mW under the 8-nm continuous tuning over each supermode observed in SG tunable twin-guide (SG-TTG) DFB TLDs [47], [48] is mainly due to the large spectral variation of the end loss in the DFB cavity which varies between 23 and 60 cm^{-1} over the tuning range. Our results also give new physical explanation of a superior performance of these widely tunable

multisection TLDs. Due to advanced design of tuning sections, the required tuning currents are considerably smaller than in a 3-section TLD. This in turn results in weak IVBA losses in the grating section due to smaller injected carrier densities.

More directly our theory is applied to recent experimental results on a widely tunable 2-section InGaAsP/InP DBR TLD with a bulk AR reported in [49]. The TLD was tuned by 13 nm with the output power decreasing from 16 to 11 mW under the maximum tuning current of 140 mA. The power drop was explained by the FCA loss in the DBR tuning section. However, the FCA effect in 1.55-μm InGaAsP/InP lasers is known to be very small [18], and thus it cannot be the cause of the power drop. According to our model, the most likely reason of the power decrease is a combination of all mechanisms considered here: the IVBA losses in the DBR section, the CRB effect in the AR, and the mutual positioning of the net gain and mirror loss spectra during the tuning. The AR gain peak in [49] was around 1530 nm and the laser was tuned over 13 nm between 1542 and 1529 nm, i.e. practically the whole wavelength tuning range corresponded to the ascending part of the material gain spectrum. The fact that the output power was decreasing with tuning indicates that both the CRB and IVBA effects were playing a key role in the TLD's power response (see Fig. 19, green line).

Another interesting application of the obtained results on the IVBA effect in the DBR section is its possible utilisation for the enhanced modulation performance of directly modulated lasers exploiting the detuned loading and photon-photon resonance effects in the DBR cavities [51]–[53]. As was shown in [52] and [53], for fixed wavelength DBR lasers the impact of a certain amount of built-in optical losses in the Bragg grating can significantly improve the modulation bandwidth and the chirp of the laser. Our results demonstrate a new physical mechanism by which the required dispersive optical losses in the grating region of multi-section laser can be externally tuned to the necessary level via the IVBA effect. This mechanism allows the optimisation of the dynamic performance of directly modulated TLD under wavelength tuning. Some preliminary results were recently obtained by us in [42], where the effect of wavelength tuning on the small-signal response was investigated, and in [54] where the enhanced small- and large-signal modulation dynamic response and spectral characteristics improvement (frequency chirping suppression) of optically-injected TLDs have been demonstrated.

VI. Conclusions

The obtained simulation results demonstrate that quite subtle but robust physical effects, such as the IVBA and the CRB as well as the mutual positioning of the net gain $g_{net}(\lambda)$ and the cavity mirror loss $\alpha_m(\lambda)$ spectra with respect to the lasing cavity mode during tuning have a strong impact on the tuning performance of TLDs in terms of the lasing wavelength range and the output power variation. This also indicates the existence of rich design options in the practical development of real TLD devices. However, these options strongly depend on particular values of the physical parameters in question in the studied laser structure. These parameters must be properly

evaluated prior to the TLD's design and optimisation in order to meet specific performance requirements.

In all of our simulations we use realistic values of the IVBA and CRB parameters which have been observed experimentally in various InP-based laser structures. By considering the range of these parameters, we practically cover all possible situations in real lasers. In fixed-wavelength lasers the actual IVBA parameters are usually evaluated via the fitting procedure, as in [55]–[57] for example, and rarely by direct absorption measurements [40]. In TLDs this procedure becomes more complex, as it is necessary to evaluate the effect of the IVBA in the passive sections on the wavelength tuning, from where the IVBA data can be acquired.

The main limitations of the TLD models simulated here include the Lorentzian lineshape approximation and neglect the heating effects due to hot-carriers, recombination, and self-heating in all sections. A self-consistent incorporation of these features into the device-level simulations is very challenging, paticularly for multisection TLDs. This is because the changes of the carrier density and/or temperature in any part of the composite cavity affect the lineshape, the gain, and the local refractive index, i.e. the power and the wavelength tuning performance of a CW TLD. A special fitting procedure (which differs from the one used in fixed-wavelength lasers [18], [34]) is also required in the case of TLDs, in order to extract the thermal parameters of the device to be used in the simulations. Such self-consistent device-level modelling tools which incorporate the above features are currently not available.

The considered models and the approaches can be further extended to more complex integrated multi-section lasers.

REFERENCES

[1] Y. Suematsu, "Dynamic single-mode lasers," *J. Lightw. Technol.*, vol. 32, no. 6, pp. 1144–1158, Mar. 15, 2014.

[2] J. Buus and E. J. Murphy, "Tunable lasers in optical networks," *J. Lightw. Technol.*, vol. 24, no. 1, pp. 5–11, Jan. 2006.

[3] L. A. Coldren, G. A. Fish, Y. Akulova, J. S. Barton, L. Johansson, and C. W. Coldren, "Tunable semiconductor lasers: A tutorial," *J. Lightw. Technol.*, vol. 22, no. 1, pp. 193–202, Jan. 2004.

[4] N. P. Caponio et al., "Analysis and design criteria of three-section DBR tunable lasers," *IEEE J. Sel. Areas Commun.*, vol. 8, no. 6, pp. 1203–1213, Aug. 1990.

[5] S. L. Woodward, U. Koren, B. I. Miller, M. G. Young, M. A. Newkirk, and C. A. Burrus, "A DBR laser tunable by resistive heating," *IEEE Photon. Technol. Lett.*, vol. 4, no. 12, pp. 1330–1332, Dec. 1992.

[6] T. Kameda et al., "A DBR laser employing passive-section heaters, with 10.8 nm tuning range and 1.6 MHz linewidth," *IEEE Photon. Technol. Lett.*, vol. 5, no. 6, pp. 608–610, Jun. 1993.

[7] S. Sakano, A. Oka, and N. Chinone, "Wavelength-tunable three-electrode DBR laser with a thin-active layer in tuning regions," *IEEE Photon. Technol. Lett.*, vol. 3, no. 10, pp. 866–868, Oct. 1991.

[8] A. A. M. Staring et al., "Wavelength-independent output power from an injection-tunable DBR laser," *IEEE Photon. Technol. Lett.*, vol. 6, no. 2, pp. 147–149, Feb. 1994.

[9] M. Teshima, "Dynamic wavelength tuning characteristics of the 1.5-μm three-section DBR lasers: Analysis and experiment," *IEEE J. Quantum Electron.*, vol. 31, no. 8, pp. 1389–1400, Aug. 1995.

[10] D. Delprat, A. Ramdane, L. Silvestre, A. Ougazzaden, F. Delorme, and S. Slempkes, "20-Gb/s integrated DBR laser-EA modulator by selective area growth for 1.55-μm WDM applications," *IEEE Photon. Technol. Lett.*, vol. 9, no. 7, pp. 898–900, Jul. 1997.

[11] V. I. Feies and I. Montrosset, "Design of two-section DBR laser operating at ITU frequencies only by grating current tuning," *J. Lightw. Technol.*, vol. 21, no. 6, pp. 1524–1530, Jun. 2003.

[12] S. L. Woodward, I. M. I. Habbab, T. L. Koch, and U. Koren, "The side-mode-suppression ratio of a tunable DBR laser," *IEEE Photon. Technol. Lett.*, vol. 2, no. 12, pp. 854–856, Dec. 1990.

[13] Y. Kotaki and H. Ishikawa, "Wavelength tunable DFB and DBR lasers for coherent optical fibre communications," *IEE Proc. J. Optoelectron.*, vol. 138, no. 2, pp. 171–177, Apr. 1991.

[14] A. Tsigopoulos, T. Sphicopoulos, I. Orfanos, and S. Pantelis, "Wavelength tuning analysis and spectral characteristics of three-section DBR-laser," *IEEE J. Quantum Electron.*, vol. 28, no. 2, pp. 415–426, Feb. 1992.

[15] G. Kyritsis, O. Duzgol, and N. Zakhleniuk, "Power and wavelength tuning performance of multi-quantum-well and bulk tunable laser diodes and main limiting factors," in *Proc. 25th Int. Semiconductor Laser Conf.*, Kobe, Japan, 2016, pp. 1–2.

[16] *PICS3D User Guide*, Crosslight Software, Burnaby, BC, Canada, 2010.

[17] J. Piprek, P. Abraham, and J. E. Bowers, "Cavity length effects on internal loss and quantum efficiency of multiquantum-well lasers," *IEEE J. Sel. Topics Quantum Electron.*, vol. 5, no. 3, pp. 643–647, May/Jun. 1999.

[18] J. Piprek, P. Abraham, and J. E. Bowers, "Self-consistent analysis of high-temperature effects on strained-layer multiquantum-well InGaAsP-InP lasers," *IEEE J. Quantum Electron.*, vol. 36, no. 3, pp. 366–374, Mar. 2000.

[19] G. Kyritsis and N. Zakhleniuk, "Self-consistent simulation model and enhancement of wavelength tuning of InGaAsP/InP multisection DBR laser diodes," *IEEE J. Sel. Topics Quantum Electron.*, vol. 19, no. 5, pp. 1–11, Sep./Oct. 2013.

[20] M. Asada and Y. Suematsu, "Density-matrix theory of semiconductor lasers with relaxation broadening model-gain and gain-suppression in semiconductor lasers," *IEEE J. Quantum Electron.*, vol. QE-21, no. 5, pp. 434–442, May 1985.

[21] M. Yamada, H. Ishiguro, and H. Nagato, "Estimation of the intra-band relaxation time in undoped AlGaAs injection laser," *Jpn. J. Appl. Phys.*, vol. 19, no. 1, pp. 135–142, 1980.

[22] M. Asada, A. Kameyama, and Y. Suematsu, "Gain and intervalence band absorption in quantum-well lasers," *IEEE J. Quantum Electron.*, vol. QE-20, no. 7, pp. 745–753, Jul. 1984.

[23] E. Zielinski, H. Schweizer, S. Hausser, R. Stuber, M. Pilkuhn, and G. Weimann, "Systematics of laser operation in GaAs/AlGaAs multi-quantum well heterostructures," *IEEE J. Quantum Electron.*, vol. QE-23, no. 6, pp. 969–976, Jun. 1987.

[24] M. Takeshima, "Theory of the carrier-carrier and carrier-phonon interactions under double injection into undoped quantum wells and its application to a laser problem," *Phys. Rev. B, Condens. Matter*, vol. 36, no. 36, pp. 8082–8093, 1987.

[25] M. Yamada et al., "Polarization-dependent gain in GaAs/AlGaAs multi-quantum-well lasers: Theory and experiment," *Appl. Phys. Lett.*, vol. 45, no. 4, pp. 324–325, 1984.

[26] M. Asada, "Intraband relaxation effect on optical spectra," in *Quantum Well Lasers*, P. S. Zory, Ed. Boston, MA, USA: Academic, 1993, ch. 2.

[27] L. A. Coldren, S. W. Corzine, and M. L. Masanovic, *Diode Lasers and Photonic Integrated Circuits*, 2nd ed. Hoboken, NJ, USA: Wiley, 2012.

[28] M. Yamanishi and Y. Lee, "Phase dampings of optical dipole moments and gain spectra in semiconductor lasers," *IEEE J. Quantum Electron.*, vol. QE-23, no. 4, pp. 367–370, Apr. 1987.

[29] S. R. Chinn, P. S. Zory, and A. R. Reisinger, "A model for GRIN-SCH-SQW diode lasers," *IEEE J. Quantum Electron.*, vol. 24, no. 11, pp. 2191–2214, Nov. 1988.

[30] A. I. Kucharska and D. J. Robbins, "Lifetime broadening in GaAs-AlGaAs quantum well lasers," *IEEE J. Quantum Electron.*, vol. 26, no. 3, pp. 443–448, Mar. 1990.

[31] M. Asada, "Intraband relaxation time in quantum-well lasers," *IEEE J. Quantum Electron.*, vol. 25, no. 9, pp. 2019–2026, Sep. 1989.

[32] M. N. Akram et al., "The effect of barrier composition on the vertical carrier transport and lasing properties of 1.55-μm multiple quantum-well structures," *IEEE J. Quantum Electron.*, vol. 42, no. 7, pp. 713–724, Jul. 2006.

[33] S. Adachi, *Physical Properties of III–V Semiconductor Compounds*. New York, NY, USA: Wiley, 1992.

[34] J. Piprek, J. K. White, and A. J. Springthorpe, "What limits the maximum output power of long-wavelength AlGaInAs/InP laser diodes?" *IEEE J. Quantum Electron.*, vol. 38, no. 9, pp. 1253–1259, Sep. 2002.

[35] B. R. Bennett, R. A. Soref, and J. A. Del Alamo, "Carrier-induced change in refractive index of InP, GaAs, and InGaAsP," *IEEE J. Quantum Electron.*, vol. 26, no. 1, pp. 113–122, Jan. 1990.

[36] J.-P. Weber, "Optimization of the carrier-induced effective index change in InGaAsP waveguides—Application to tunable Bragg filters," *IEEE J. Quantum Electron.*, vol. 30, no. 8, pp. 1801–1816, Aug. 1994.

[37] Y. Suematsu and S. Arai, "Single-mode semiconductor lasers for long-wavelength optical fiber communications and dynamics of semiconductor lasers," *IEEE J. Sel. Topics Quantum Electron.*, vol. 6, no. 5, pp. 1436–1449, Nov./Dec. 2000.

[38] J. Buus, M.-C. Amann, and D. J. Blumenthal, *Tunable Laser Diodes and Related Optical Sources*, 2nd ed. Hoboken, NJ, USA: Wiley, 2005.

[39] S. Kakimoto and H. Watanabe, "Intervalence band absorption loss coefficients of the active layer for InP-based long wavelength laser diodes," *J. Appl. Phys.*, vol. 87, no. 5, pp. 2095–2097, Mar. 2000.

[40] C. H. Henry, R. A. Logan, F. R. Merritt, and J. P. Luongo, "The effect of intervalence band absorption on the thermal behavior of InGaAsP lasers," *IEEE J. Quantum Electron.*, vol. QE-19, no. 6, pp. 947–952, Jun. 1983.

[41] *VPIcomponentMaker Photonic Circuits*, VPIphotonics, Berlin, Germany, 2015.

[42] O. Duzgol, G. Kyritsis, and N. Zakhleniuk, "Travelling-wave modelling of the modulation dynamic performance of wavelength-tunable laser diodes using the integrated VPI and PICS3D software," *IET Optoelectron.*, vol. 11, no. 2, pp. 66–72, 2017, doi: 10.1049/iet-opt.2016.0067.

[43] M. Yamada, S. Ogita, M. Yamagishi, and K. Tabata, "Anistropy and broadening of optical gain in a GaAs/AlGaAs multiquantum-well laser," *IEEE J. Quantum Electron.*, vol. QE-21, no. 6, pp. 640–645, Jun. 1985.

[44] A. J. Ward *et al.*, "Widely tunable DS-DBR laser with monolithically integrated SOA: Design and performance," *IEEE J. Sel. Topics Quantum Electron.*, vol. 11, no. 1, pp. 149–156, Jan./Feb. 2005.

[45] L. Ponnampalam *et al.*, "Equivalent performance in *C*- and *L*-bands of digital supermode distributed Bragg reflector lasers," *IEEE J. Quantum Electron.*, vol. 43, no. 9, pp. 798–803, Sep. 2007.

[46] Y. A. Akulova *et al.*, "Widely tunable electroabsorption-modulated sampled-grating DBR laser transmitter," *IEEE J. Sel. Topics Quantum Electron.*, vol. 8, no. 6, pp. 1349–1357, Nov. 2002.

[47] R. Todt *et al.*, "Sampled grating tunable twin-guide laser diodes with over 40-nm electronic tuning range," *IEEE Photon. Technol. Lett.*, vol. 17, no. 12, pp. 2514–2516, Dec. 2005.

[48] R. Todt, T. Jacke, R. Meyer, R. Laroy, G. Morthier, and M. C. Amann, "Widely tunable twin-guide laser diodes with sampled gratings: Design and performance," *IEEE J. Sel. Topics Quantum Electron.*, vol. 13, no. 5, pp. 1095–1103, Sep. 2007.

[49] L. Yu *et al.*, "Widely tunable narrow-linewidth lasers using self-injection DBR lasers," *IEEE Photon. Technol. Lett.*, vol. 27, no. 1, pp. 50–53, Jan. 1, 2015.

[50] H. Ishii, H. Tanobe, F. Kano, Y. Tohmori, Y. Kondo, and Y. Yoshikuni, "Quasicontinuous wavelength tuning in super-structure-grating (SSG) DBR lasers," *IEEE J. Quantum Electron.*, vol. 32, no. 3, pp. 433–441, Mar. 1996.

[51] U. Feise, "Optimization of modulation bandwidth in DBR lasers with detuned Bragg reflector," *IEEE J. Quantum Electron.*, vol. 34, no. 12, pp. 2371–2379, Dec. 1998.

[52] P. Bardella and I. Montrosset, "A new design procedure for DBR lasers exploiting the photon–photon resonance to achieve extended modulation bandwidth," *IEEE J. Sel. Topics Quantum Electron.*, vol. 19, no. 4, pp. 1095–1103, Jul./Aug. 2013.

[53] M. Chacinski and R. Schatz, "Impact of losses in the Bragg section on the dynamics of detuned loaded DBR lasers," *IEEE J. Quantum Electron.*, vol. 46, no. 9, pp. 1360–1367, Sep. 2010.

[54] O. Duzgol, G. Kyritsis, and N. Zakhleniuk, "Enhanced dynamic response and spectral characteristics improvement of optically-injected widely-tunable laser diodes," in *Proc. 25th Int. Semiconductor Laser Conf.*, Kobe, Japan, 2016, pp. 1–2.

[55] A. P. Mozer, S. Hauser, and M. H. Pilkuhn, "Quantitative evaluation of gain and losses in quaternary lasers," *IEEE J. Quantum Electron.*, vol. QE-21, no. 6, pp. 725–791, Jun. 1985.

[56] I. Joindot and J. L. Beylat, "Intervalence band absorption coefficient measurements in bulk layer, strained and unstrained multiquantum well 1.55 μm semiconductor lasers," *Electron. Lett.*, vol. 29, no. 7, pp. 604–605, Apr. 1993.

[57] D. A. Ackerman *et al.*, "Analysis of gain in determining T_0 in 1.3 μm semiconductor lasers," *IEEE J. Sel. Topics Quantum Electron.*, vol. 1, no. 2, pp. 250–263, Jun. 1995.

Georgios Kyritsis received the B.Sc. degree in informatics and telecommunications from the National and Kapodistrian University of Athens, Athens, Greece, in 2007, and the M.Sc. degree in telecommunications and information systems and the Ph.D. degree in computing and electronic systems from the University of Essex, Colchester, U.K., in 2008 and 2015, respectively. He is currently a Research Officer with the School of Computer Science and Electronic Engineering, University of Essex. His research interests include the use of tunable laser diodes in high-speed long-haul optical networks.

Nick Zakhleniuk received the M.Sc. degree from National Technical University, Kyiv, Ukraine, in 1978, and the Ph.D. degree in condensed matter theory from the Institute of Semiconductor Physics, NASU, Kyiv, in 1984. From 1994 to 1996, he was a Royal Society Post-Doctoral Fellow with the University of Essex, Colchester, U.K., where he was involved in the theory of low-dimensional semiconductors. From 2000 to 2003, he was a Senior Scientist with Marconi Optical Components and Bookham Technology, Caswell, U.K., where he was involved in research on photonic and microelectronic devices and components. Since 2003, he has been with the University of Essex. He has authored over 100 papers and four collective monographs, and holds seven international patents on optoelectronic and photonic devices.